

Ising Meson Spectroscopy on a Noisy Digital Quantum Simulator

Christopher Lamb,^{*} Yicheng Tang, Robert Davis, and Ananda Roy[†]
Department of Physics and Astronomy, Rutgers University, Piscataway, NJ 08854-8019 USA

Quantum simulation has the potential to be an indispensable technique for the investigation of non-perturbative phenomena in strongly-interacting quantum field theories (QFTs). In the modern quantum era, with Noisy Intermediate Scale Quantum (NISQ) simulators widely available and larger-scale quantum machines on the horizon, it is natural to ask: what non-perturbative QFT problems can be solved with the existing quantum hardware? We show that existing noisy quantum machines can be used to analyze the energy spectrum of a large family of strongly-interacting 1+1D QFTs. The latter exhibit a wide-range of non-perturbative effects like ‘quark confinement’ and ‘false vacuum decay’ which are typically associated with higher-dimensional QFTs of elementary particles. We perform quench experiments on IBM’s `ibmq_mumbai` quantum simulator to compute the energy spectrum of 1+1D quantum Ising model with a longitudinal field. The latter model is particularly interesting due to the formation of mesonic bound states arising from a confining potential for the Ising domain-walls, reminiscent of t’Hooft’s model of two-dimensional quantum chromodynamics. Our results demonstrate that digital quantum simulation in the NISQ era has the potential to be a viable alternative to numerical techniques such as density matrix renormalization group or the truncated conformal space methods for analyzing QFTs.

Investigation of non-perturbative phenomena in strongly interacting quantum field theories (QFTs) remains one of the outstanding challenges of modern physics. Despite impressive progress, ab-initio lattice computations of properties of arbitrary QFTs will likely remain beyond the computational capabilities of the most powerful classical computer. This is due to the exponentially-growing Hilbert space which poses an insurmountable challenge for exact simulation of these lattice models. Nevertheless, quasi-exact or approximate classical computing techniques have been successful in investigating a large family of quantum many-body systems that realize QFTs in the scaling limit. For example, states with ‘relatively low entanglement’ can be efficiently represented using tensor networks [1–4]. This has allowed high-precision investigation of low-energy states of one-dimensional, local, gapped and gapless Hamiltonians using matrix product states [5] as well as their two-dimensional generalizations [6–8].

Despite the success of classical computing methods, simulation of high-energy states or non-equilibrium dynamics remains challenging even for generic, strongly-interacting 1+1D quantum systems. This is due to the rapid growth of entanglement between different subsystems [9–12]. Quantum simulation, both analog and digital, have the potential to become a viable alternative to the aforementioned approaches for tackling these questions [13, 14]. Analog quantum simulation involves tailoring a given quantum system to emulate a specific target model [15–20] and has been remarkably successful in analyzing a wide range of physical problems. However, it is gate-based, error-corrected, digital quantum simulation that is the long-term, universal solution for simulation of QFTs [21]. In this approach, lattice regularizations of QFTs can be encoded into registers of error-corrected qubits with suitable initial state preparation, time evo-

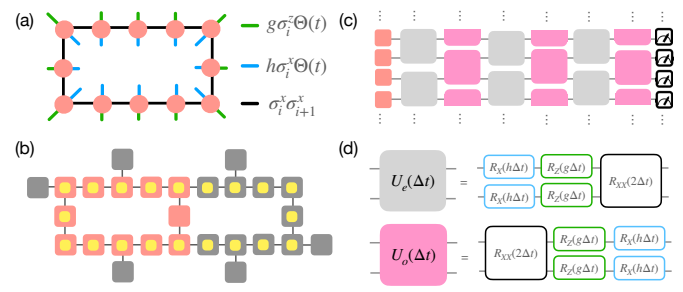


FIG. 1. (a) Schematic of the periodic Ising chain. The coral circles indicate spin-1/2 sites. The black, green and blue bonds respectively correspond to the ferromagnetic interaction, transverse and longitudinal fields respectively. The quench protocol considered in this work involves turning on the longitudinal and transverse field strengths: $g \leq 1, h < 1$ in the Hamiltonian of Eq. (1) after preparing the system in the ground state of H with $g = h = 0$: $|\rightarrow, \dots, \rightarrow\rangle$. (b) Schematic of the qubit layout in IBM’s `ibmq_mumbai` quantum simulator. Of the available 27 qubits (in gray), a periodic chain of 12 qubits (in coral) and 20 qubits (in yellow) were chosen for the quench experiments. (c) Schematic of the trotterized unitary time-evolution generated by the Hamiltonian H . The action of the full unitary operator is decomposed into the unitary operators: U_e and U_o . At the end of the time-evolution, single qubit measurements are performed in the σ_y basis. (d) The decompositions of U_e and U_o in terms of single and two qubit gates are shown.

lution and measurement protocols. To that end, protocols for digitization of scalar fields [22, 23] and quantum algorithms for computation of scattering processes in scalar [24] and fermionic [25] QFTs have already been proposed.

However, implementing such a quantum simulation protocol on existing quantum hardware remains a daunting challenge. In spite of the recent progress in the fab-

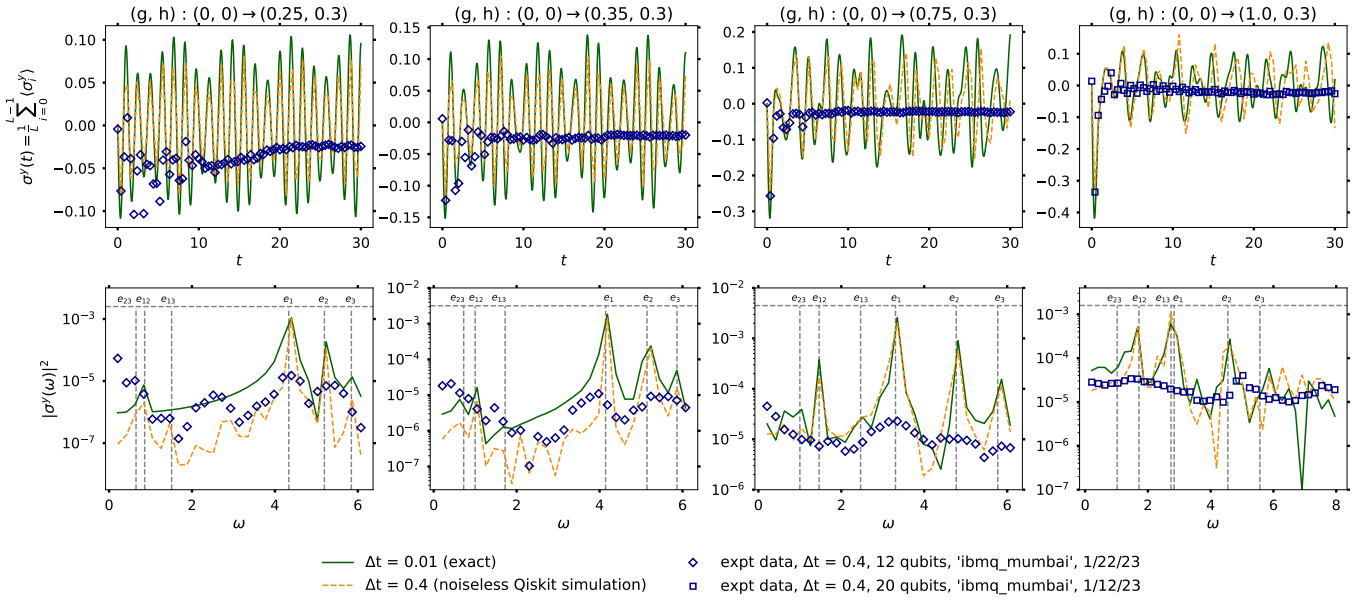


FIG. 2. Ising meson spectroscopy simulation and experimental results for quench from $g = h = 0$. The Qiskit twirled readout error extinction and dynamical decoupling schemes were used to mitigate the effects of noise present in the IBM Mumbai simulator. (Top panels) Results for $\sigma^y(t) = \sum_j \langle \sigma_j^y(t) \rangle / L$ for different quench parameters are shown. A periodic chain with length $L = 12$ (20) qubits [in pink (yellow) in Fig. 1] was used for quenches to $g < 1 (= 1)$ with $h = 0.3$. The results obtained using exact simulation of the time evolution of L qubits with $\Delta t = 0.01$ are shown with green solid lines. The noiseless numerical Qiskit simulation results are performed for $\Delta t = 0.4$ (orange dashed line). The expectation values for the noiseless simulations are computed by trotterized time-evolution and making measurements in the σ^y basis for each qubit after every time-step and averaging over 8192 shots. The close agreement of the noiseless simulation and the exact results confirm the relatively low trotterization error for $\sigma^y(t)$ even for the quench to $g = 1$. The experimental data from the quantum hardware (IBM Mumbai) are shown as blue diamonds (squares) for $g < 1 (= 1)$. (Bottom panels) The squared absolute values of the Fourier transforms $\sigma^y(\omega)$ are shown. The peaks in the latter correspond to the rest energies (e_n), of the mesonic excitations labeled by n , and their differences (e_{mn}). The gray dashed lines correspond to the exact diagonalization results obtained in the zero momentum sector.

lication and manipulation photonic and solid-state systems, the number of available qubits across the different quantum computing platforms remains around 10^2 with modest coherence times. Given the large overhead in the number of required qubits to implement quantum error correcting codes [26], it is an open problem to implement error-corrected digital simulation of QFTs in the near term. This raises the question: *what non-perturbative QFT problems can be tackled with current Noisy Intermediate Scale Quantum (NISQ) machines?*

In this work, a superconducting NISQ simulator is used to compute the energy spectra of certain strongly-interacting QFTs that arise as scaling limits of one-dimensional quantum spin chains. The latter QFTs offer a valuable playground for investigation of a wide range of non-perturbative phenomena such as ‘quark confinement’ [27] and ‘false vacuum decay’ [28] that are typically associated with QFTs in higher-dimensions. Importantly, there are two practical advantages: i) these spin-chains can be directly mapped to arrays of qubits without additional overhead involved in discretizing the local lattice degree of freedom, ii) several properties of

these spin-chains can be investigated with existing classical numerical techniques (tensor networks) and analytical methods (Bethe ansatz and bosonization). This enables benchmarking NISQ simulators before using them for investigation of problems that truly lie beyond the reach of the classical computers.

The goal of this work is to demonstrate the aforementioned using the paradigmatic example of the one-dimensional quantum Ising model in the presence of a longitudinal field [29]. The Hamiltonian is:

$$H = - \sum_{j=1}^L (\sigma_j^x \sigma_{j+1}^x + g \sigma_j^z + h \sigma_j^x), \quad (1)$$

where g, h are the strengths of the transverse and longitudinal fields and we have chosen periodic boundary conditions. We consider the case $g \leq 1, h < 1$. The presence of the longitudinal field introduces a confining potential between the domain-wall excitations of the Ising model. This leads to formation of ‘mesonic’ bound states, analogous to hadron-formation in quantum chromodynamics [30]. The energy spectrum has been analyzed using semi-classical [31, 32], truncated conformal space [33–36]

and exact diagonalization [37] approaches. While signatures of confinement have been observed for this model in a NISQ simulator [38] (see also Ref. [39] for analysis of a related model), digital quantum simulation of the energy spectrum has remained elusive. This is performed in this work using a quench experiment on IBM's `ibmq_mumbai` (hereafter referred to as IBM Mumbai) simulator which is one of the IBM Quantum Falcon Processors. The quantum simulation protocol is first tested using the Qiskit software package [40] and benchmarked against exact computations. Subsequently, it is implemented on the noisy quantum hardware.

The quantum simulation protocol is as follows (see Fig. 1). First, the qubits are prepared in the state: $|\rightarrow, \dots, \rightarrow\rangle$, which is one of the two degenerate ground state of the Hamiltonian H with $g = h = 0$ [41]. This is done by applying a Hadamard gate on each qubit after initializing them in the ground state. Next, a global quench is performed to $0 < g \leq 1, h < 1$. The quench experiments with $g < 1$ ($= 1$) were performed on a 12 (20) qubit loop [in pink (yellow) in Fig. 1] within the IBM Mumbai simulator. The quench is implemented in the NISQ hardware by the application of single and two-qubit gates (see Fig. 1(c,d) for the gate decomposition) [42] that together give rise to the unitary operator $U = e^{-iH\Delta t}$. Here, Δt is the size of the time-step. The rest energy spectrum of the mesonic excitations formed due to the confinement of fermionic Ising domain-walls manifests itself in the observables that involve only single-qubit operators [37]. This is particularly suitable for implementation in a NISQ machine where single qubit measurements are performed with relatively low error. In particular, in this work, the single-qubit observable $\langle \sigma_j^y(t) \rangle$, j being the site-index, is measured during the course of this evolution [43].

Fig. 2 shows the results for the quenches from $g = h = 0$ to $g \leq 1, h = 0.3$. The top panels show the measured variation of $\sigma^y(t) = \sum_j \langle \sigma_j^y(t) \rangle / L$ with time. The solid green curves act as reference and are obtained from exact computation of the time-evolution of the chain of qubits with $\Delta t = 0.01$ [44]. The dashed orange curves are obtained from numerical simulations on a noiseless Qiskit simulator for $\Delta t = 0.4$. In this case, the expectation value $\langle \sigma_j^y(t) \rangle$ was computed for each qubit at each time-step by measuring it in the corresponding basis and averaging over 8192 shots. The close agreement of the noiseless simulation results for the two choices of Δt indicates a small trotterization error for this observable. The quantum simulation experiment on IBM Mumbai was performed with the same parameters as the noiseless simulations. The experimental data is shown as blue diamonds (squares) for $g < 1 (= 1)$. To mitigate the effects of errors and noise on the quantum hardware, the in-built Qiskit twirled readout error extinction and dynamical decoupling schemes were chosen. The bottom panels show the absolute values of the corresponding Fourier trans-

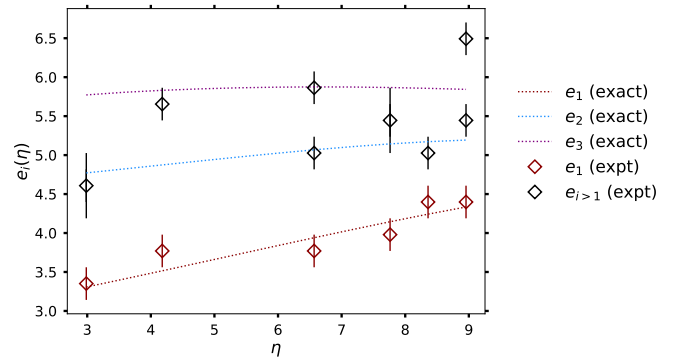


FIG. 3. Variation of the meson energies obtained from quantum simulation experiments performed on the IBM Mumbai simulator. The results (in diamonds) are shown for a quench from $g = h = 0$ to $g \in [0.25, 0.75]$ and $h = 0.3$. The corresponding predictions from exact diagonalization of the 12-site qubit chain keeping only the translation-invariant states are shown as dotted lines. The meson energies are shown as a function of the dimensionless parameter $\eta = 2\pi(1-g)/h^{8/15}$. The peaks for the different meson energies were identified by computing the $\sigma^y(\omega)$ for quenching to different choices of g [see also Fig. 2]. Notice that the obtained quantum data did not always permit unambiguous identification of the second and third meson energies. Nevertheless, the agreement between the experimentally obtained lowest meson energy and the exact diagonalization results is reasonable.

forms. The rest energies of the mesons are inferred from the location of the peaks, with the dashed vertical lines being results obtained using exact diagonalization in the zero momentum sector. Note that the quality of the data from the quantum hardware for $g = 1$ is worse than the $g < 1$ cases. This is due to the lower gap between the ground and first excited states of the energy spectrum. This makes the experiments more susceptible to the noise arising due to trotterization and noise in the IBM Mumbai simulator. Nevertheless, the peak corresponding to the difference between the lowest two meson energies is clearly discernible for the $g = 1$ case.

Fig. 3 shows the variation of the meson energies obtained from different quench experiments performed on the IBM Mumbai simulator. In every experiment, the system was initialized in the ground state of $g = h = 0$. Subsequently, a quench was performed to $h = 0.3$ and g varying between 0.25 and 0.75 in steps of 0.05. The obtained meson energies are shown as diamonds. The corresponding predictions from the exact diagonalization of the qubit chain in the zero momentum sector are shown as dotted lines. Notice that the noisy data did not always permit unique identification of the second and third meson energies. However, the lowest meson energy could always be unambiguously obtained. The agreement between the experimentally-obtained lowest meson energies and the exact diagonalization results is reasonable.

Fig. 4 shows the results for the connected correla-

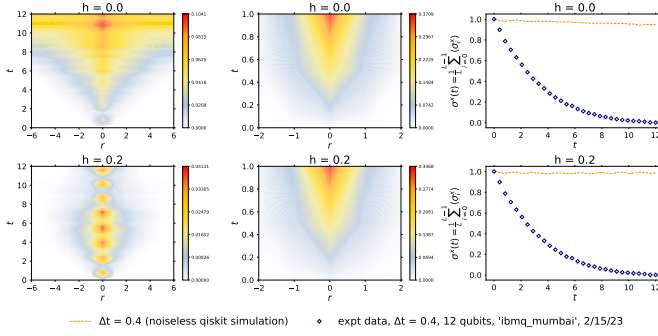


FIG. 4. Results for $G_x(r, t)$ and the $\langle \sigma^x(t) \rangle$ for a quench to $g = 0.25, h = 0$ and $g = 0.25, h = 0.3$. The noiseless simulation results for $G_x(r, t)$ are shown in the left panels. The corresponding results for $\langle \sigma^x(t) \rangle$ are shown with orange dashed lines in the right panels. The simulation parameters are the same as in Fig. 2. The results of the quantum simulation experiments on the IBM Mumbai simulator are shown in the middle panel and with blue diamonds in the right panel. With the current noisy gates and qubits on the quantum hardware, a distinct signature of confinement could not be discerned. This is consistent with the rapid decay of $\langle \sigma^x(t) \rangle$ (blue diamonds in the right panels). Additional error mitigation techniques and improved quantum hardware can be used to obtain more reliable signatures of the confinement in the correlation functions.

tion function $G_x(r, t) = \langle \sigma_i^x(t) \sigma_{i+r}^x(t) \rangle - \langle \sigma_i^x(t) \rangle \langle \sigma_{i+r}^x(t) \rangle$. The latter contains signatures of the confinement of the domain-walls into mesonic excitations [37]. The results of the noiseless Qiskit simulations are shown in the left panels. The simulation parameters are kept as in Fig. 2. For $h = 0$, the correlation function exhibits a characteristic broadening due to the propagation of the energy-carrying domain wall excitations [9] until the separation between the latter is of the order of the system size (top left panel). For $h \neq 0$, as the domain-walls get separated, they feel the confining force that leads to the formation of the mesonic bound states. This results in oscillatory behavior of the correlation function [37] (bottom left panel). The corresponding expectation value $\sigma^x(t) = \sum_j \langle \sigma_j^x(t) \rangle / L$ for the noiseless simulations are shown with the dashed orange line in the right panels. The data from the quantum hardware is shown in the middle panels. With the current noise levels in the gates and modest lifetimes of the qubits of IBM's Mumbai simulator, signatures of confinement could not be reliably discerned for the noisy experimental data for the correlation function. This is consistent with the measured rapid decay of $\sigma^x(t)$ shown with blue diamonds in the right panel (compare the oscillations obtained for $\langle \sigma^y(t) \rangle$ shown in Fig. 2). Additional error mitigation techniques and improved quantum hardware could be used to obtain signatures of confinement in the correlation functions.

In summary, this work highlights the potential of NISQ simulators for investigation of non-perturbative problems

in strongly-interacting QFTs. In particular, a noisy IBM simulator is used to compute the energy-spectrum of the mesonic excitations occurring in the one-dimensional Ising model with a longitudinal field. These mesonic excitations have masses that are larger than twice the mass of the Ising domain walls [29]. This leads to a correlation length that is even smaller than the ordinary gapped, Ising model in the ferromagnetic phase, making this model particularly suitable for realization on a NISQ simulator.

The demonstrated quantum simulation scheme can be straightforwardly generalized to analyze a wide family of 1+1D QFTs. A natural extension is the quantum sine-Gordon model perturbed by a cosine potential with a twice the periodicity. This model can be realized as the scaling limit of the XYZ spin chain [45] in the presence of a longitudinal field. In the latter model, the free Ising domain walls are replaced by interacting sine-Gordon solitons [46–49]. For details of the simulation protocol and noiseless simulations results at the free-fermion point of the latter model, see [50]. With improved noise properties, larger sizes, and more sophisticated error-mitigation techniques that are likely to be available in the coming years, it is conceivable that a wider range of QFTs will become amenable to quantum simulation on quantum hardware in the imminent future.

The authors acknowledge discussions with Nicholas Bronn, Robert Konik and Olivia Lanes and the use of IBM Quantum services for this work. The views expressed are those of the authors, and do not reflect the official policy or position of IBM or the IBM Quantum team. AR was supported from a grant from the Simons Foundation (825876, TDN).

* cdl92@physics.rutgers.edu

† ananda.roy@physics.rutgers.edu

- [1] M. B. Hastings, An area law for one-dimensional quantum systems, *J. Stat. Mech.* **0708**, P08024 (2007), [arXiv:0705.2024 \[quant-ph\]](https://arxiv.org/abs/0705.2024).
- [2] G. Vidal, Class of quantum many-body states that can be efficiently simulated, *Phys. Rev. Lett.* **101**, 110501 (2008).
- [3] N. Schuch, M. M. Wolf, F. Verstraete, and J. I. Cirac, Entropy scaling and simulability by matrix product states, *Phys. Rev. Letters* **100**, [10.1103/physrevlett.100.030504](https://doi.org/10.1103/physrevlett.100.030504) (2008).
- [4] F. Verstraete, V. Murg, and J. Cirac, Matrix product states, projected entangled pair states, and variational renormalization group methods for quantum spin systems, *Advances in Physics* **57**, 143 (2008).
- [5] U. Schollwöck, The density-matrix renormalization group in the age of matrix product states, *Annals of Physics* **326**, 96 (2011), january 2011 Special Issue.
- [6] F. Verstraete and J. I. Cirac, *Renormalization algorithms for quantum-many body systems in two and higher dimensions* (2004).

[7] N. Schuch, M. M. Wolf, F. Verstraete, and J. I. Cirac, Computational complexity of projected entangled pair states, *Phys. Rev. Lett.* **98**, 140506 (2007).

[8] M. P. Zaletel and F. Pollmann, Isometric tensor network states in two dimensions, *Phys. Rev. Lett.* **124**, 037201 (2020).

[9] P. Calabrese and J. Cardy, Evolution of entanglement entropy in one-dimensional systems, *Journal of Statistical Mechanics: Theory and Experiment* **2005**, P04010 (2005).

[10] G. Vidal, Classical simulation of infinite-size quantum lattice systems in one spatial dimension, *Phys. Rev. Lett.* **98**, 070201 (2007).

[11] S. Paeckel, T. Köhler, A. Swoboda, S. R. Manmana, U. Schollwöck, and C. Hubig, Time-evolution methods for matrix-product states, *Annals of Physics* **411**, 167998 (2019).

[12] S.-H. Lin, M. P. Zaletel, and F. Pollmann, Efficient simulation of dynamics in two-dimensional quantum spin systems with isometric tensor networks, *Phys. Rev. B* **106**, 10.1103/physrevb.106.245102 (2022).

[13] R. P. Feynman, Simulating Physics with Quantum Computers, *International Journal of Theoretical Physics* **21**, 467 (1982).

[14] S. Lloyd, Universal Quantum Simulators, *Science* **273**, 1073 (1996).

[15] B. Douçot, L. B. Ioffe, and J. Vidal, Discrete non-abelian gauge theories in josephson-junction arrays and quantum computation, *Phys. Rev. B* **69**, 214501 (2004).

[16] J. I. Cirac, P. Maraner, and J. K. Pachos, Cold atom simulation of interacting relativistic quantum field theories, *Phys. Rev. Lett.* **105**, 190403 (2010).

[17] H. P. Büchler, M. Hermele, S. D. Huber, M. P. A. Fisher, and P. Zoller, Atomic quantum simulator for lattice gauge theories and ring exchange models, *Phys. Rev. Lett.* **95**, 040402 (2005).

[18] J. Casanova, L. Lamata, I. L. Egusquiza, R. Gerritsma, C. F. Roos, J. J. García-Ripoll, and E. Solano, Quantum simulation of quantum field theories in trapped ions, *Phys. Rev. Lett.* **107**, 260501 (2011).

[19] C. Gross and I. Bloch, Quantum simulations with ultracold atoms in optical lattices, *Science* **357**, 995 (2017), <https://science.sciencemag.org/content/357/6355/995.full.pdf>.

[20] A. Roy and H. Saleur, Quantum electronic circuit simulation of generalized sine-gordon models, *Phys. Rev. B* **100**, 155425 (2019).

[21] S. P. Jordan, K. S. M. Lee, and J. Preskill, Quantum Algorithms for Quantum Field Theories, *Science* **336**, 1130 (2012), [arXiv:1111.3633 \[quant-ph\]](https://arxiv.org/abs/1111.3633).

[22] A. Macridin, P. Spentzouris, J. Amundson, and R. Harnik, Digital quantum computation of fermion-boson interacting systems, *Phys. Rev. A* **98**, 10.1103/physreva.98.042312 (2018).

[23] N. Klco and M. J. Savage, Digitization of scalar fields for quantum computing, *Phys. Rev. A* **99**, 10.1103/physreva.99.052335 (2019).

[24] S. P. Jordan, K. S. M. Lee, and J. Preskill, Quantum Computation of Scattering in Scalar Quantum Field Theories, *Quant. Inf. Comput.* **14** (2014), [arXiv:1112.4833 \[hep-th\]](https://arxiv.org/abs/1112.4833).

[25] S. P. Jordan, K. S. M. Lee, and J. Preskill, Quantum Algorithms for Fermionic Quantum Field Theories, (2014), [arXiv:1404.7115 \[hep-th\]](https://arxiv.org/abs/1404.7115).

[26] M. A. Nielsen and I. L. Chuang, *Quantum Computation and Quantum Information* (Cambridge University Press, 2000).

[27] J. Greensite, *An introduction to the confinement problem*, Vol. 821 (2011).

[28] S. Coleman, *Aspects of Symmetry: Selected Erice Lectures* (Cambridge University Press, 1988).

[29] B. M. McCoy and T. T. Wu, Two-dimensional ising field theory in a magnetic field: Breakup of the cut in the two-point function, *Phys. Rev. D* **18**, 1259 (1978).

[30] G. 't Hooft, A two-dimensional model for mesons, *Nuclear Physics B* **75**, 461 (1974).

[31] S. B. Rutkevich, Large- n excitations in the ferromagnetic ising field theory in a weak magnetic field: Mass spectrum and decay widths, *Phys. Rev. Lett.* **95**, 250601 (2005).

[32] S. B. Rutkevich, Energy spectrum of bound-spinons in the quantum ising spin-chain ferromagnet, *J. Stat. Phys.* **131**, 917 (2008).

[33] P. Fonseca and A. Zamolodchikov, Ising field theory in a magnetic field: Analytic properties of the free energy, *J. Stat. Phys.* **110**, 527 (2003).

[34] P. Fonseca and A. Zamolodchikov, Ising spectroscopy. I. Mesons at $T < T_c$, (2006), [arXiv:hep-th/0612304](https://arxiv.org/abs/hep-th/0612304).

[35] A. J. A. James, R. M. Konik, and N. J. Robinson, Non-thermal states arising from confinement in one and two dimensions, *Phys. Rev. Lett.* **122**, 130603 (2019).

[36] N. J. Robinson, A. J. A. James, and R. M. Konik, Signatures of rare states and thermalization in a theory with confinement, *Phys. Rev. B* **99**, 195108 (2019).

[37] M. Kormos, M. Collura, G. Takács, and P. Calabrese, Real-time confinement following a quantum quench to a non-integrable model, *Nature Physics* **13**, 246 (2016).

[38] J. Vovrosh and J. Knolle, Confinement and entanglement dynamics on a digital quantum computer, *Scientific Reports* **11**, 11577 (2021).

[39] W. L. Tan, P. Becker, F. Liu, G. Pagano, K. S. Collins, A. De, L. Feng, H. B. Kaplan, A. Kyprianidis, R. Lundgren, W. Morong, S. Whitsitt, A. V. Gorshkov, and C. Monroe, Domain-wall confinement and dynamics in a quantum simulator, *Nature Physics* **17**, 742 (2021).

[40] A. tA-v et al, *Qiskit: An open-source framework for quantum computing* (2021).

[41] The protocol could be implemented also with the initial state being the ground state of the Hamiltonian with $g < 1, h = 0$. However, preparing such an initial state on a quantum simulator is nontrivial [51, 52]. For simplicity, we restrict ourselves to initial product states.

[42] A. Smith, M. S. Kim, F. Pollmann, and J. Knolle, Simulating quantum many-body dynamics on a current digital quantum computer, *npj Quantum Inf.* **5**, 106 (2019), [arXiv:1906.06343 \[quant-ph\]](https://arxiv.org/abs/1906.06343).

[43] The meson energy spectrum can be also computed by measuring $\langle \sigma_j^x(t) \rangle$ or $\langle \sigma_j^z(t) \rangle$. On a noisy simulator, the best noise-resilience for mass computation was obtained for $\langle \sigma_j^y(t) \rangle$. The same choice was found to be optimal with regards to the errors arising from trotterization of the continuous time-evolution.

[44] Exact simulation of $g = 1$ with 20 qubits was challenging for the classical computational resources available for this work. This case was computed with Qutip [53, 54].

[45] R. Baxter, *Exactly Solved Models in Statistical Mechanics*, Dover Books on Physics (Dover Publications, 2013).

[46] G. Delfino and G. Mussardo, Non-integrable aspects of the multi-frequency sine-gordon model, *Nuclear Physics*

B **516**, 675–703 (1998).

[47] Z. Bajnok, L. Palla, G. Takacs, and F. Wagner, Nonperturbative study of the two frequency sine-Gordon model, *Nucl. Phys. B* **601**, 503 (2001), [arXiv:hep-th/0008066](https://arxiv.org/abs/hep-th/0008066).

[48] G. Mussardo, V. Riva, and G. Sotkov, Semiclassical particle spectrum of double sine-Gordon model, *Nucl. Phys. B* **687**, 189 (2004), [arXiv:hep-th/0402179](https://arxiv.org/abs/hep-th/0402179).

[49] A. Roy and S. Lukyanov, Soliton Confinement in a Quantum Circuit, arXiv (2023), [arXiv:2302.06289 \[quant-ph\]](https://arxiv.org/abs/2302.06289).

[50] See supplementary material for details.

[51] F. Verstraete, J. I. Cirac, and J. I. Latorre, Quantum circuits for strongly correlated quantum systems, *Phys. Rev. A* **79**, 032316 (2009).

[52] W. W. Ho and T. H. Hsieh, Efficient variational simulation of non-trivial quantum states, *SciPost Phys.* **6**, 029 (2019).

[53] J. Johansson, P. Nation, and F. Nori, Qutip: An open-source python framework for the dynamics of open quantum systems, *Computer Physics Communications* **183**, 1760 (2012).

[54] J. Johansson, P. Nation, and F. Nori, Qutip 2: A python framework for the dynamics of open quantum systems, *Computer Physics Communications* **184**, 1234 (2013).